Atomic-scale characterization of single and double layers of InAs and InAlAs Stranski-Krastanov quantum dots

Raja Sekhar Reddy Gajjela [1,*] Ahmad Alzeidan [2] Victor M. O. Curbelo [2] Alain A. Quivy [2] and Paul M. Koenraad [1]

[1]*Department of Applied Physics and Science Education, Eindhoven University of Technology, Eindhoven 5612 AZ, The Netherlands*

[2]*Institute of Physics, University of São Paulo, Rua do Matão 1371, 05508-090 São Paulo, SP, Brazil*

(Received 14 September 2022; accepted 15 November 2022; published 30 November 2022)

We report a detailed structural characterization of single and double layers of InAs and InAlAs quantum dots (QDs) and their wetting layers (WLs) by atomic force microscopy (AFM) and cross-sectional scanning tunneling microscopy (X-STM). The X-STM analysis with atomic resolution showed that the InAlAs WL consists of two distinct layers: a bottom part where all the Al atoms of the InAlAs alloy settled, and a top part containing exclusively In and Ga atoms. The QDs formed from the InAlAs layer contains no Al atoms at all and lie on top of the Al-rich WL. In the double layers of QDs, the InAlAs QDs were used as a seed to influence the nucleation of the InAs QDs grown on top. A gradual decrease in the density of the top InAs QDs was observed in the AFM images with increasing thickness of the GaAs spacer. The X-STM images showed that both QDs layers were completely intermixed for a 2-nm-thick spacer, while effective strain-induced stacking of both types of QDs was observed for a GaAs spacer thickness of 4 nm. However, both QD layers were completely decoupled for a GaAs spacer thickness of 8 nm and could thus be treated as individual layers.

DOI: 10.1103/PhysRevMaterials.6.114604

I. INTRODUCTION

Quantum dots (QDs) are of great interest as they represent an ideal system to investigate the confinement of carriers in all three spatial dimensions and provide novel properties for many optoelectronic applications such as semiconductor lasers [1], infrared photodetectors [2], intermediate-band solar cells [3], ultrahigh-density optical memories [4], flash memories [5,6], quantum computing and information [7–11], etc. When dealing with solid-state devices, the InAs/GaAs system is often used because homogeneous three-dimensional (3D) InAs islands can be easily nucleated on the GaAs(001) surface using the Stranski-Krastanov (SK) growth mode which involves the strain-induced formation of 3D islands due to the lattice mismatch between the two materials [12]. However, well before this self-assembling process, Ga atoms from the substrate are incorporated into the growing InAs film in an attempt to reduce the strain [13], leading thus to the growth of InGaAs layers instead [14]. During the capping process, the increasing strain—which changes from biaxial to hydrostatic—drives the indium atoms from the apex of the QDs to the sides, leading to a stronger In-Ga intermixing and resulting in smaller QDs containing even less indium [15].

Self-assembled SKQDs are simple to grow and easily monitored *in situ* using the reflection high-energy electron diffraction (RHEED) technique. Since their formation is strain driven, they can be obtained using several epitaxial techniques and different materials [16,17]. Although SK growth rapidly became a major growth technique to produce high-quality QDs for solid-state devices, it has some drawbacks such as a limited degree of freedom to control the QDs size and density, as well as the presence of a two-dimensional (2D) wetting layer (WL) in direct contact with the QDs which contributes to the strain and reduces the 3D confinement of the carriers. However, the major problem is probably their relatively low surface density, usually around 1–5 $\times$ 10^{10} cm^{-2}. Several ways to increase the density of QDs were suggested, like the deposition of multiple SKQDs layers [18] or the use of the submonolayer technique to form a different type of QDs [19,20]. The former does not increase their areal (2D) density but rather increases their bulk (3D) density, raising thus the elastic energy stored in the system. The latter can achieve a much higher surface density, supposedly in the low 10^{12} cm^{-2} range, and provide an easy way to control their height, but the deposition is more complex, time consuming, and the growth conditions still need optimization [21–23].

Another method to increase the QDs density consists of depositing AlGaAs layers just below the InAs QDs. The deposition of InAs QDs on an AlAs surface allows an increase in density up to 10^{11} cm^{-2} due to the reduced surface diffusion of the In atoms on an Al-rich surface [24]. However, the QDs are smaller and their optical emission is shifted towards shorter wavelengths. A different way to use Al atoms was proposed by Kovsh *et al.* [25] who suggested the growth of InAlAs SKQDs instead of InAs. The addition of Al to the alloy to be deposited can increase the density of QDs by roughly an order of magnitude due to the low mobility of the Al atoms on the GaAs(001) surface, thus increasing the number of nucleation centers. Here again the density of InAlAs QDs is higher than for common InAs QDs, they have a smaller size, and their emission is blueshifted as well. One drawback is that their optical activity is limited, as they have a shallow ground state when embedded in a GaAs matrix [26],

*r.s.r.gajjela@tue.nl

and barrier materials with a larger band gap are required to improve their optical properties. InAlAs layers have already been extensively investigated when lattice matched to InP substrates ($In_{0.52}Al_{0.48}As$), as it can serve as a barrier to lattice-matched $In_{0.53}Ga_{0.47}As$ [27], but it can also be used as a metamorphic buffer on GaAs substrates [28] for device applications. However, there are only sporadic studies about InAlAs QDs grown on GaAs [29–33], and just a few more about InAlAs layers used as a barrier or confinement layer for InAs QDs deposited on GaAs [34,35].

Due to the above-mentioned properties, InAlAs QDs can be used as a seed layer to induce a larger density of conventional InAs QDs grown just on top of them. Since the seed layer and the top QDs layer can have their growth conditions adjusted independently, a high density of InAs QDs with a wide range of sizes can be achieved [36]. Recently, Claro *et al.* [26] used InAlAs QDs as a seed layer to increase the density of InAs QDs in quantum-dot infrared photodetectors (QDIPs). They observed an intense photovoltaic effect that was attributed to the strong asymmetry of the conduction band resulting most probably from the accumulation of Al atoms in the WL which turned into a potential barrier for electrons. Although their transmission electron microscopy (TEM) measurements could barely resolve the very small InAlAs QDs, they inferred from band-structure calculations and photoluminescence (PL) spectra that the InAlAs QDs consisted approximately of $In_{0.5}Ga_{0.5}As$. This is of course counterintuitive as it is a common belief that InAlAs QDs can reach a higher density because they are supposed to contain Al atoms [25]. It is very important to know precisely the morphology and composition of those nanostructures at the atomic level if one wishes to correctly simulate their optoelectronic properties.

In this work, InAlAs QDs deposited on GaAs were investigated by atomic force microscopy (AFM), cross-sectional scanning tunneling microscopy (X-STM), and photoluminescence (PL). We gave special attention to the position of the Al atoms in the WL and QDs, and we provided an estimation of their concentration in both regions via finite element (FE) simulations. We finally evaluated the influence of InAlAs-QDs seed layers on the nucleation of InAs QDs grown just on top of them by changing the thickness of the GaAs spacers.

II. EXPERIMENTAL TECHNIQUES

All the samples analyzed in this work were grown by molecular beam epitaxy (MBE) on a GaAs(001) substrate. The first sample was grown specifically on a Si-doped GaAs(001) substrate (doping concentration $n = 1 \times 10^{18}$ cm^{-3}) for X-STM measurements. After oxide removal and degassing of the substrate at 610 °C for 5 min, a 200-nm-thick Si-doped GaAs buffer ($n = 1 \times 10^{18}$ cm^{-3}) was deposited at 570 °C. Then the temperature was lowered to 515 °C and the following layers were grown to form the structure shown in Fig. 1. Layer 1: 1.40 MLs of InAs were deposited to simulate an InAs WL. Layer 2: 2.30 MLs of $In_{0.7}Al_{0.3}As$ were deposited to simulate an InAlAs WL. Layers 3 and 4: InAs and $In_{0.7}Al_{0.3}As$ SKQDs were grown by depositing 2.0 MLs of InAs and 3.5 MLs of InAlAs, respectively, to obtain isolated nanostructures that will be used as a reference and compared with the double layers of QDs that follow. Layers 5 to 7: Double layers of $In_{0.7}Al_{0.3}As$ and InAs QDs were grown by changing the thickness (X) of the GaAs spacer, i.e., $X = 2$ nm for layer 5, $X = 4$ nm for layer 6, and $X = 8$ nm for layer 7. Each layer (and double layers) was separated from the others by 200 nm of GaAs, in which the central part (120 nm) was Si doped to provide good conductivity for the X-STM measurements. The InAs and $In_{0.7}Al_{0.3}As$ QDs layers were deposited at 0.088 and 0.128 ML s^{-1}, respectively, while the growth rate of the GaAs material was 1.0 ML s^{-1} throughout the sample. The QDs formation was monitored *in situ* using the RHEED technique which confirmed that all $In_{0.7}Al_{0.3}As$ QDs were always formed after deposition of 2.5 MLs of material. The critical thickness of the InAs QDs was 1.7 MLs for the single layer of QDs (layer 3) but was systematically reduced in the double layers having smaller GaAs spacers (down to 0.7 ML for the 2 nm spacer). Each InAs or $In_{0.7}Al_{0.3}As$ layer was covered by 15 nm of GaAs deposited at 515 °C to avoid In desorption, followed by 185 nm of GaAs grown at 570 °C. The growth of the first two layers of interest (layers 1 and 2) was stopped before QDs formation to allow a detailed study of the original WL. The following two single layers of QDs (layers 3 and 4) were used to investigate uncoupled QDs, whereas the last three layers (layers 5 to 7) provided information about the influence of the seed layer in double layers of QDs with different spacer thickness.

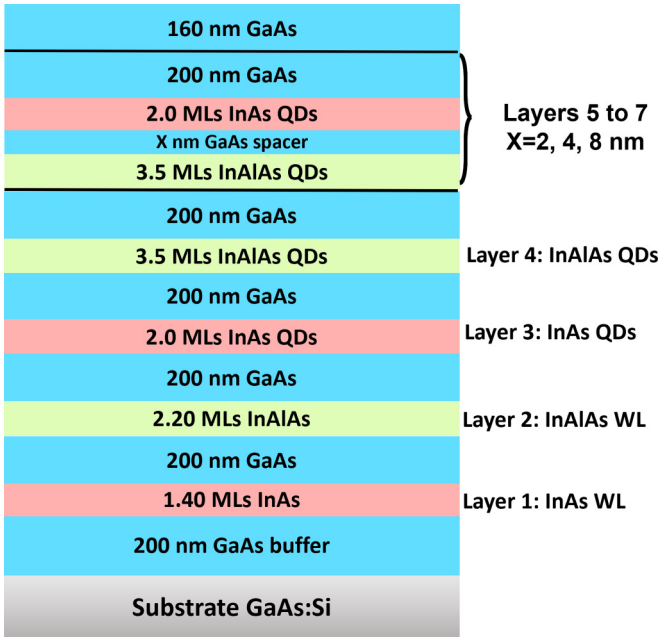

FIG. 1. Schematic structure of the sample grown by molecular beam epitaxy for the X-STM experiments.

The second set of seven samples containing each of the different combinations of $In_{0.7}Al_{0.3}As$ and/or InAs layers mentioned above was also grown to assess their optical properties individually. The same combinations of layers were replicated at the surface of each sample to measure the QDs density in the top layer by AFM. All these samples had a similar structure and were grown in the same conditions explained before, with two slight differences: no Si doping

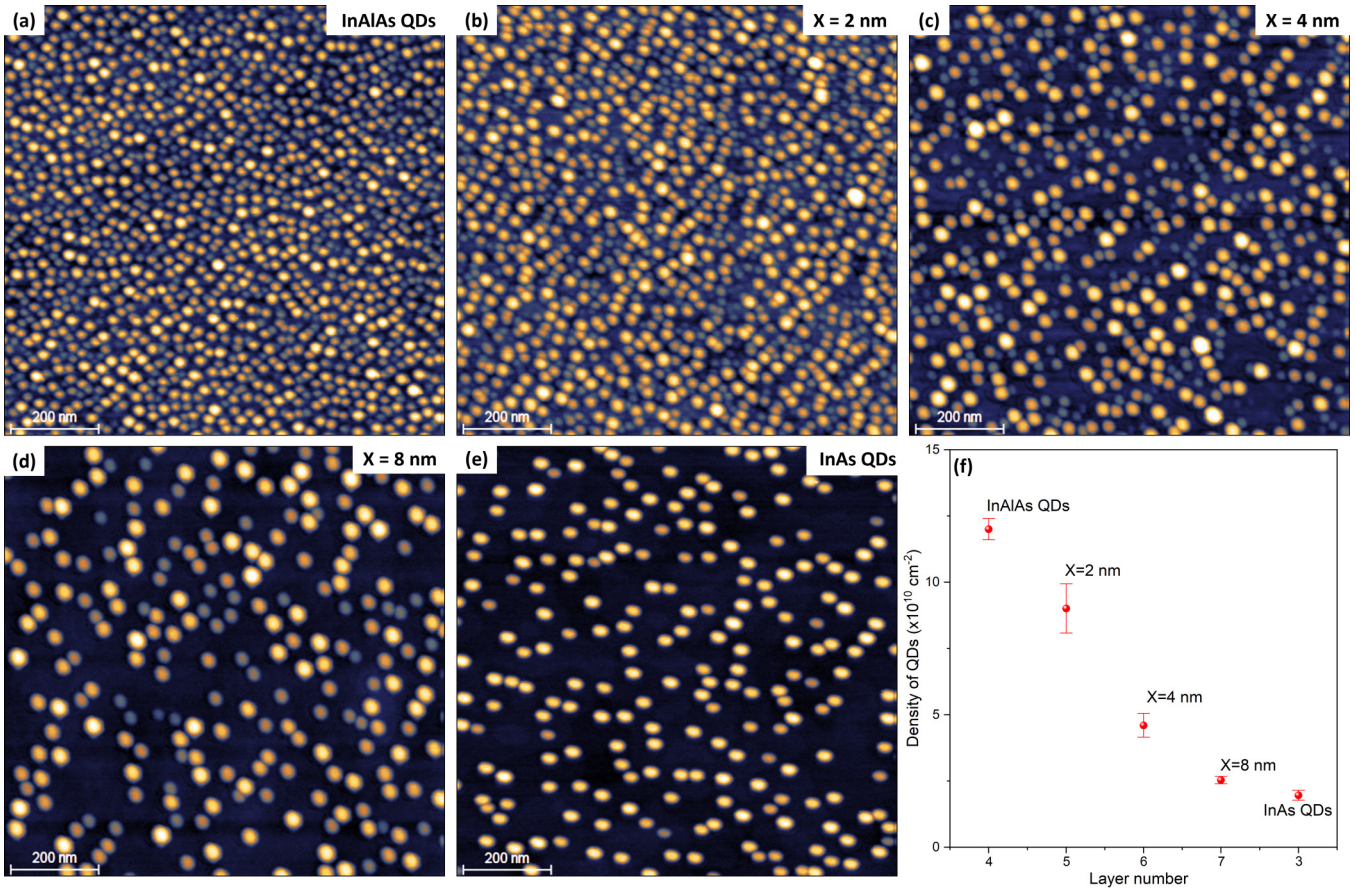

FIG. 2. $1 \times 1\ \mu m^2$ AFM images showing the density of uncapped QDs in each layer: (a) InAlAs QDs, layer 4. (b) Double QDs layers with a 2 nm GaAs spacer, layer 5. (c) 4 nm GaAs spacer, layer 6. (d) 8 nm GaAs spacer, layer 7. (e) InAs QDs, layer 3. The decrease in density of QDs from (a) to (e) is shown in (f). The density of QDs in layer 7 (with 8 nm spacer) is almost the same as in a single layer of InAs QDs (layer 3), indicating the absence of mechanical coupling between the top InAs QDs and the InAlAs seed layer underneath.

was used anywhere, and the GaAs layer separating the buried structures from the top ones was only 100 nm thick. The PL measurements were carried out at liquid-nitrogen temperature using a 100 mW solid-state laser emitting at 660 nm and a silicon detector. The AFM measurements were performed in ambient conditions with an Icon scanning probe microscope from Bruker operating in intermittent-contact mode with a Si_3N_4 probe.

All the X-STM measurements were performed in a conventional Omicron low-temperature STM at liquid-nitrogen temperature (77 K) under ultrahigh vacuum (UHV, 4–6 $\times$ 10^{-11} mbar) on the first sample containing all the seven layers of interest. The measurements were carried out on a clean {110} surface freshly obtained by cleaving the sample in UHV. The STM tips were made of polycrystalline tungsten wires by electrochemical etching followed by baking and Ar sputtering inside the STM preparation chamber under UHV. All the X-STM images of the QDs were acquired in constant current mode. Due to the atomic arrangement of the {110} surfaces of zincblende crystals, only every second monolayer along the growth direction is visible in the X-STM images. Therefore, in the present case, either the group-III or group-V atoms can be observed at a time, meaning that an atomic row actually represents a bilayer (BL) [37]. For filled-state imaging at high negative bias voltages, the group-V sublattice (As) was imaged, while in empty-state imaging at positive bias voltages, the group-III sublattice (Al, Ga, In) was imaged. FE simulations were performed using the structural mechanics module on COMSOL: Multiphysics and the constructed QD model was based on the structural analysis performed by X-STM.

III. RESULTS AND DISCUSSION

The structural characterization of the QDs started with AFM measurements being performed on the surface QDs layers of the second set of samples. In Fig. 2(a) one can notice the very high density (1.3×10^{11} cm^{-2}) of a single layer of $In_{0.7}Al_{0.3}As$ QDs, layer 4 with relatively smaller QDs (3 nm high and 10 nm wide), whereas a single layer of standard InAs QDs, layer 3 [Fig. 2(e)] has a much lower density (2.0×10^{10} cm^{-2}) of QDs with a comparatively larger size (7 nm high and 20 nm wide). This increase in density by a factor of 6 for the InAlAs QDs is generally attributed to the lower surface mobility of the Al atoms [25,26,38]. Figures 2(b)–2(d) show that, when these $In_{0.7}Al_{0.3}As$ QDs are used as a seed layer, they are able to increase the density of InAs QDs in the top layer up to 9.0×10^{10} cm^{-2} when their separation is only 2 nm [layer 5, Fig. 2(b)], and to 4.7×10^{10} cm^{-2} when the spacer is 4 nm thick [layer 6, Fig. 2(c)]. For an

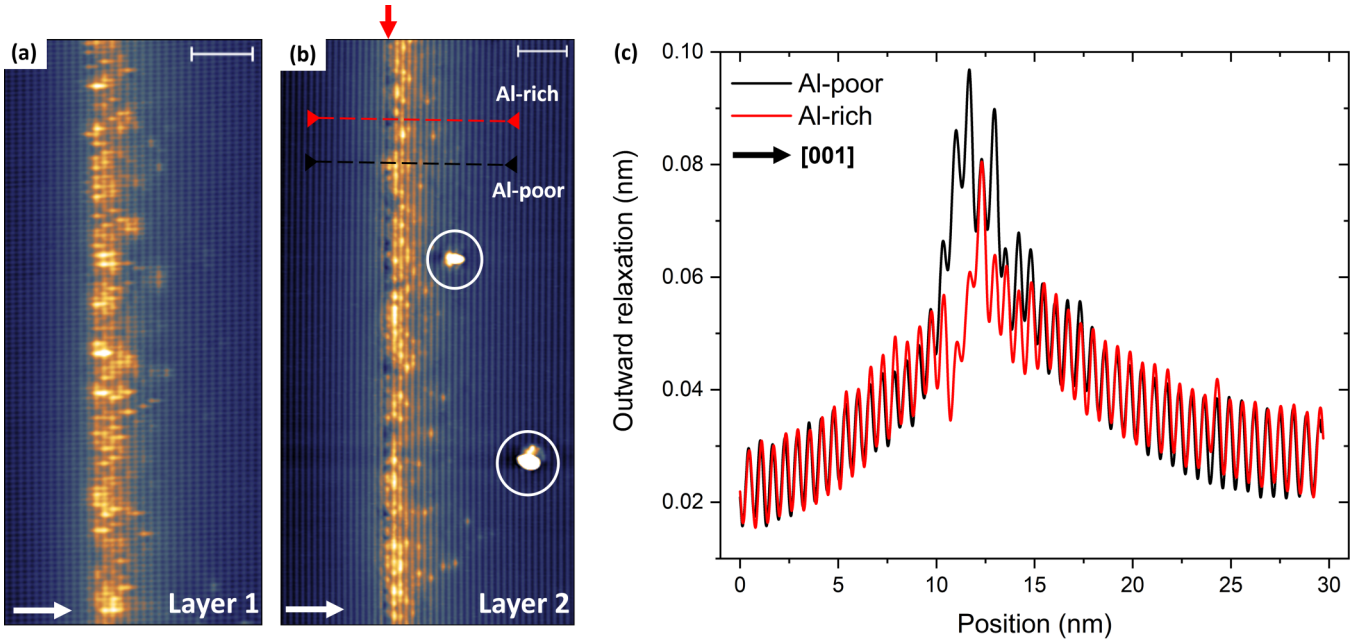

FIG. 3. X-STM filled-state topographic images comparing the formation of the WLs in layer 1, InAs WL (a) and layer 2, InAlAs WL (b) taken at a bias voltage (V_b) = −3.0 V and tunnel current (I_t) = 50 pA. The bottom-most atomic layer in (b), indicated with a red arrow, reveals the dark areas corresponding to the presence of Al, indicating that the deposited Al settled at the bottom of the WL. The color contrast from dark to bright represents a height difference of 0 to 100 pm. The length of the scale bar is 5 nm and the white arrow indicates the growth direction [001]. The two white circles in (b) indicate some contaminants or tip-related artifacts. Two lines indicate the position where the height profiles in (c) were taken: the black line was drawn through an Al-poor region, while the red line was drawn through an Al-rich region. The presence of Al is clearly visible in the height profile (red) as a drop in the outward relaxation of the WL.

8-nm-thick spacer [layer 7, Fig. 2(d)], it is reduced down to 2.5×10^{10} cm^{-2}, suggesting that the strain field inside the thin GaAs spacer is barely able to influence the nucleation of the InAs QDs in the top layer, and the two QDs layers are almost decoupled. AFM and X-STM measurements are complementary, as AFM allows the investigation of the sample surfaces, providing statistical information about the size, shape, and density of the QDs before capping, as well as an indication of the alignment efficiency in double layers of QDs. On the other hand, X-STM can resolve the internal structure of individual QDs with atomic resolution and provides an estimation of the size, shape, and composition of the embedded nanostructures.

Figure 3 shows X-STM filled-state topographic images of layer 1 (InAs WL) and layer 2 (InAlAs WL) with a dark-to-bright contrast representing a height difference of 0 to 100 pm. The color contrast in the images represents the relative height of the STM tip from the cleaved surface. The compressively strained InAs and InAlAs layers relaxed outwards up on cleaving, giving a bright topographic contrast as shown in Fig. 3. The filled-state imaging was performed at high negative bias voltages (−3.0 V) to suppress any electronic contribution to the images which led to a nearly pure structural contrast [39,40]. As mentioned in the sample description, 1.40 MLs of InAs were deposited in layer 1 and 2.30 MLs of $In_{0.7}Al_{0.3}As$ in layer 2; therefore, the absolute quantity of In is higher in layer 2 than in layer 1. In Fig. 3(a) layer 1 (InAs WL) appears as a dilute layer of InGaAs material with a thickness of 3–4 BLs along the growth direction. On the other hand, layer 2 (InAlAs WL) shown in Fig. 3(b) appears brighter compared to layer 1 due to the higher In content concentrated within a thickness of ∼2–3 BLs. The most interesting observation is the presence of dark patches at the bottom of the WL [indicated by the red arrow in Fig. 3(b)], which is associated with the presence of Al atoms. The two white circles in Fig. 3(b) show some contaminants or tip-related artifacts created during the measurement. It is well established that In atoms have high surface mobility, while on the contrary, Al atoms have low surface mobility and are readily incorporated into the GaAs lattice due to the absence of lattice mismatch [38,41]. Usually, Al atoms provide a dark contrast in the X-STM images mainly due to their smaller size, as already shown in previous experiments on GaAs/AlGaAs droplet epitaxy QDs [42,43]. Since the STM height profiles show the outward relaxation of the compressively strained layers, two height profiles were taken at different locations of the InAlAs WL. Figure 3(c) shows the two profiles taken through an Al-poor (black line) and an Al-rich (red line) region. At around 11–12 nm (x axis), one can observe a clear drop in the relaxation of the WL due to the presence of Al (red line). Therefore, it is safe to conclude that the Al atoms in the InAlAs WL are sitting at the bottom of the WL, while the rest of it is made of In(Ga)As. Claro *et al.* [26] suggested that the Al could be restricted to the bottom of the WL, but we are now able to provide a direct visual proof from the X-STM images, further strengthening the argument. Additionally, our X-STM data point out that the presence of Al atoms actually pins many In atoms at the sample surface, unlike what happens for the InAs WL, where the In atoms are free to segregate. Figure 4 shows topographic filled-state images of layer 3 [InAs QDs,

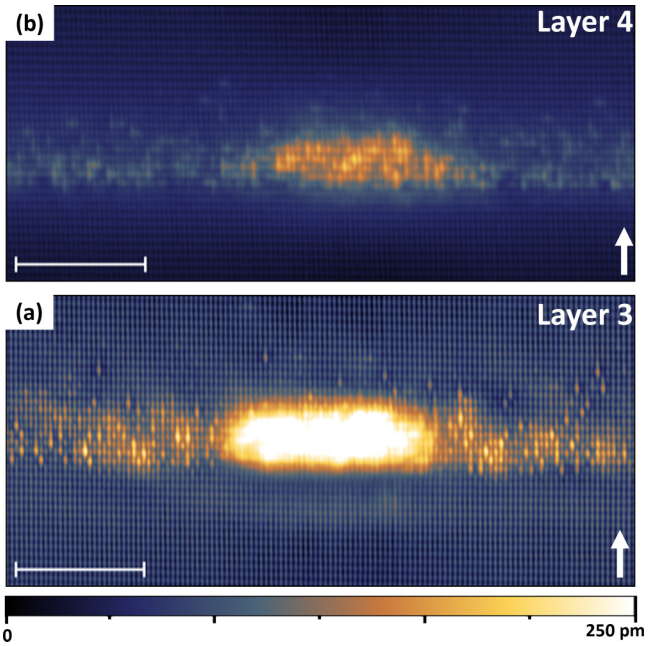

FIG. 4. X-STM filled-state topographic images comparing the InAs and InAlAs QDs in layer 3 (a) and 4 (b) taken at $V_b = -3.0$ V and $I_t = 50$ pA. The color contrast from dark to bright represents a height difference of 0 to 250 pm. The lower brightness in InAlAs QD in (b) compared to the InAs QD in (a) suggests a lower indium concentration within the QD. The length of the scale bar is 10 nm and the white arrow indicates the growth direction [001].

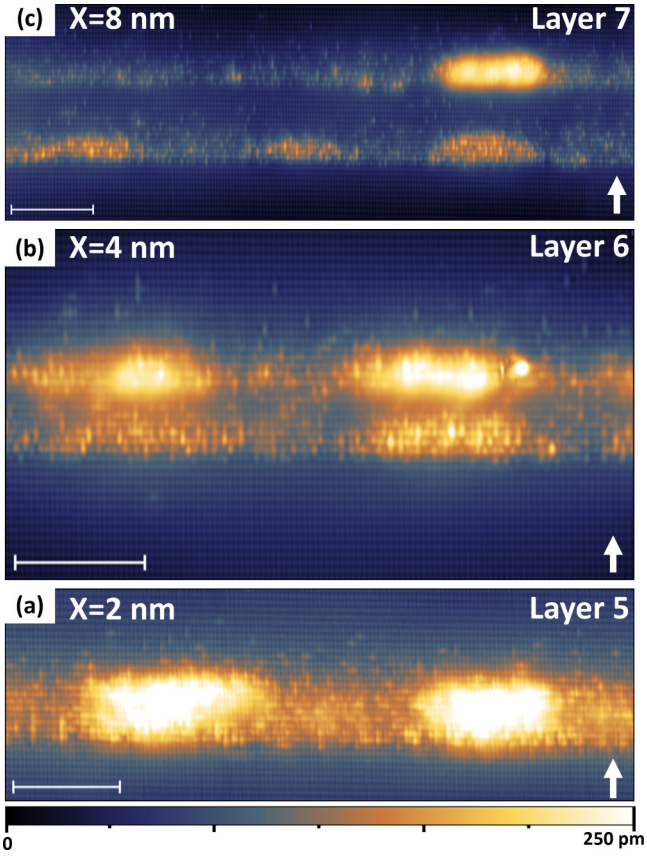

FIG. 5. X-STM filled-state topographic images showing the effect of the GaAs spacer on the formation of InAs QDs in layers 5 (a), 6 (b), and 7 (c) taken at $V_b = -3.0$ V and $I_t = 50$ pA. The InAs QDs are deposited on top of the InAlAs seed layer QDs. The color contrast from dark to bright represents a height difference of 0 to 250 pm. The intermixing and strain-induced stacking are evident in (a) and (b), respectively. The two QDs layers in (c) are already decoupled for a GaAs spacer thickness of 8 nm. The length of the scale bar is 10 nm and the white arrow indicates the growth direction [001].

Fig. 4(a)] and layer 4 [InAlAs, Fig. 4(b)] with a dark-to-bright color contrast of 0 to 250 pm. The InAs QD shown in Fig. 4(a) has a base length of 18 ± 0.8 nm and a height of 4.0 ± 0.5 nm while the InAlAs QD shown in Fig. 4(b) has a base length of 21.6 ± 0.8 nm and a height of 4.2 ± 0.5 nm. The reported dimensions are for the remnant of the QDs after cleaving. The cleaving process is completely random and does not necessarily run through the center of every single QD. Depending on the cleaving position with respect to the QD, we observe different heights and base lengths. The AFM analysis of InAlAs QDs [Fig. 2(a)] suggested a smaller height and base length compared to InAs QDs contradicting the X-STM observations. In Fig. 2(a) one can see some QD ripening, where smaller QDs coalesce into larger QDs. It is possible that the large InAlAs QD measured in Fig. 4(b) is one of the ripened InAlAs QDs with larger height and base length. Since both QDs in Fig. 4 are among the largest nanostructures that were observed, they most probably reflect their full size. From Fig. 4 both InAs and InAlAs QDs have a near trapezoidal shape, suggesting that the geometry of the QDs is a truncated pyramid in three dimensions. The major difference between the InAs and InAlAs QDs shown in Fig. 4 is the difference in image contrast which relates to the average composition of the nanostructures. A QD with high indium content is more compressively strained and provides a very bright contrast in the X-STM images. The InAlAs QD shown in Fig. 4(b) has a weak contrast, indicating that its average indium content is quite low compared to the InAs QD. In Fig. 3(b) we observed that the Al atoms were lying at the bottom of the InAlAs WL due to their low surface mobility. Once again, one can see in Fig. 4(b) that the Al atoms are restricted to the bottom part of the WL and QDs of the InAlAs layer, leading thus to QDs made of InGaAs only. It is difficult to identify the dark patches at the bottom of the QDs, as the outward relaxation of the QD dominates the contrast. However, by adjusting the contrast and examining multiple images, we can confidently confirm that the Al atoms are sitting at the bottom of the WL, and none of them can be found in the QD.

Figure 5 shows topographic X-STM images of QDs in layers 5–7 [Figs. 5(a)–5(c)] with a GaAs spacer thickness (X) of 2, 4, and 8 nm, respectively. In layer 5, for a GaAs spacer of 2 nm, both InAlAs and InAs QDs intermixed completely, forming a single large QD as shown in Fig. 5(a). The very bright contrast in the QDs region suggests a higher indium content compared to the other layers. It is difficult to assess the exact shape and size of these large QDs as both types of QDs merged and are indistinguishable. Figure 5(b) shows the topography of both InAlAs (bottom layer) and InAs QDs (top layer) in layer 6 where the GaAs spacer is 4 nm thick. In this case, the GaAs spacer is thick enough to distinguish the seed layer from the InAs QDs, and the strain-induced stacking of

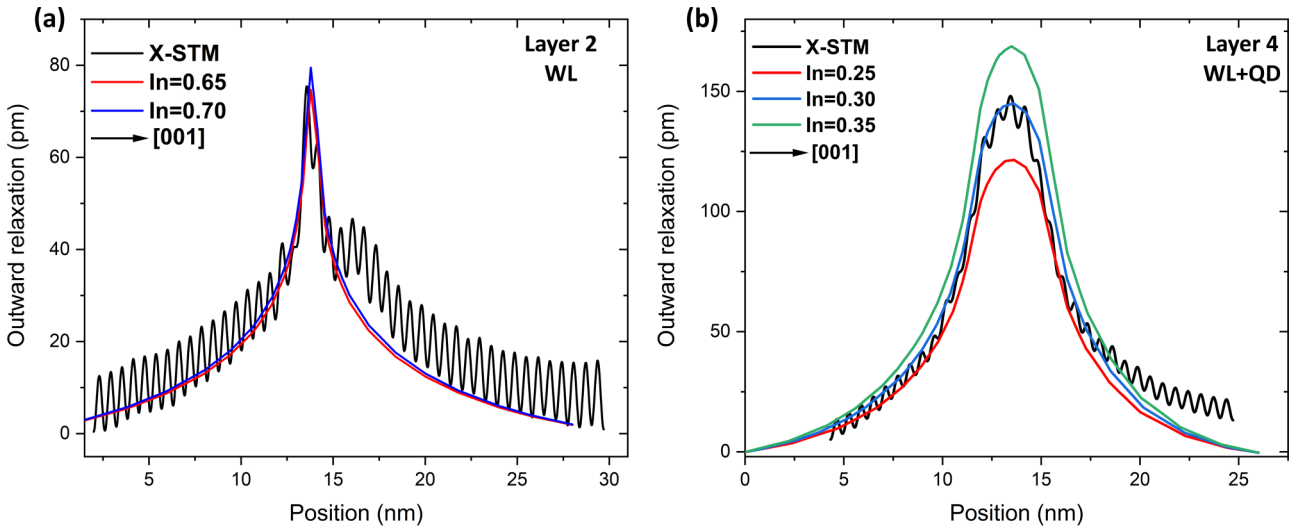

FIG. 6. (a) Experimental outward relaxation profile of the InAlAs WL from layer 2 [topographic image shown in Fig. 3(b)] measured by X-STM is shown in black and the calculated profiles for two different compositions are shown in red (In = 0.65) and blue (In = 0.70). Both measured and calculated outward relaxation profiles match very well for a 1 BL thick WL with an indium fraction of 0.65–0.70. (b) X-STM outward relaxation profile of InAlAs QD from layer 4 [topographic image shown in Fig. 4(b)] is shown in black with calculated profiles from FE simulations, red: In = 0.25, blue: In = 0.30, and green: In = 0.35. Both measured and calculated outward relaxation profiles match very well for a QD with a composition of $In_{0.30}Ga_{0.70}As$ [shown in (b)], both sitting on top of a 1 BL thick Al-rich layer ($In_{0.05–0.10}Al_{0.3}Ga_{0.60–0.65}As$).

both types of QDs can be clearly seen. Upon increasing the GaAs spacer thickness to 8 nm (layer 7), both the InAlAs QDs and InAs QDs seem to be completely decoupled with some occasional stacking of the QDs in both layers as shown in Fig. 5(c). Therefore, when the two QDs layers are separated by 8 nm (or more), both can be treated as individual layers containing InAs and InAlAs QDs as in layers 3 and 4, respectively. In Fig. 4 we observed a clear difference in contrast, suggesting that the InAlAs QDs have lower indium concentration than InAs QDs. The same argument applies to the QDs in layers 6 [Fig. 5(b)] and 7 [Fig. 5(c)], as the InAlAs QDs, have weaker contrast compared to InAs QDs. After careful examination of multiple X-STM images, we can confirm once again that the QDs of the seed layer lies on top of an Al-rich portion of the WL, as in layer 4, and there is no trace of aluminum anywhere inside the QDs in layers 5–7.

Based on Raman scattering measurements, Ibanez *et al.* [44] suggested that there could be Al/In intermixing in InAs QDs surrounded by AlGaAs, but they did not provide any direct evidence. Using the same optical technique, Sahli *et al.* [45] came to the same conclusion and inferred an even stronger Al/In intermixing when InAlAs QDs were buried in an AlGaAs matrix. However, once again, no direct evidence was provided. In our case, the InAlAs layers were surrounded by GaAs, but we have direct visual evidence at the atomic scale showing that the Al atoms remain at the bottom of the WL. The QDs themselves are formed on top of this Al-rich WL, but do not contain any Al atoms at all, are actually made of InGaAs material, as proposed by Claro *et al.* [26]. In general, cleaving the compressively strained InAs and InAlAs layers generates an outward relaxation of the surface, which strongly depends on the local composition, and can be measured by X-STM height profiles, as shown in Fig. 6. Therefore, we performed FE simulations to fit the experimental outward relaxation of the InAlAs WL (layer 2) and InAlAs QD (layer 4) with the calculated relaxation obtained via continuum elasticity theory. See the Supplemental Material [46] for a detailed explanation of the FE simulations.

From the topographic X-STM image and height profiles shown in Figs. 3(b) and 3(c), it is clear that the InAlAs WL (layer 2) mainly consists of two parts: one Al-rich layer, with a thickness of 1 BL, followed by another BL thick In-rich layer. Therefore, we performed FE simulations by constructing a model based on the X-STM characterization, where the WL composition was the only free parameter. Based on the X-STM images, two layers were created with a thickness of 1 BL each: the first layer had a composition of $In_{0.05–0.10}Al_{0.3}Ga_{0.65–0.70}As$, assuming that all the deposited Al was incorporated into the layer; the second layer had a thickness of 1 BL, and its In content was varied until the calculated relaxation matched the experimental relaxation. In Fig. 6(a) the average relaxation of the InAlAs WL measured from X-STM is shown in black together with the calculated profiles from FE simulations, where the red and blue profiles have In concentrations of 0.65 and 0.70, respectively. The small bump in the experimental relaxation profile [around 15 nm in Fig. 6(a)] is mainly due to In segregation and was neglected for the sake of simplicity. It is clear that the calculated relaxation of the WL fits very well (both the height and width of the peak) the experimental profile for a WL composition of $In_{0.05–0.10}Al_{0.3}Ga_{0.60–0.65}As$ for the 1 BL thick Al-rich layer and $In_{0.65–0.70}Ga_{0.30–0.35}As$ for the 1 BL thick In-rich layer. Therefore, the FE simulations further strengthen our arguments on the composition of the InAlAs WL, confirming that the Al atoms settled at the bottom of the WL and the top layer is mostly made of In(Ga)As.

We performed similar FE simulations on InAlAs QDs (layer 4) to provide an estimation of their composition. In

X-STM it is assumed that the largest QD is observed whenever the cleaving plane runs through the QD center. Therefore, a QD model was constructed with the dimensions of the largest InAlAs QD found during the X-STM measurement (base length = 24 nm, height = 4 nm, see the Supplemental Material [46]). From the X-STM analysis, it is clear that there is no trace of Al inside the QD, and from Fig. 4 we can infer that there is less indium in an InAlAs QD than in an InAs QD. Also, from the WL analysis, we established that the deposited Al atoms settled at the bottom of the WL. Therefore, the FE simulations were performed for a square-based truncated pyramidal QD sitting on top of a BL thick Al-rich WL ($In_{0.05–0.10}Al_{0.3}Ga_{0.60–0.65}As$), assuming that the QD was cleaved through its center. Figure 6(b) shows an experimental relaxation profile of an InAlAs QD in black together with calculated profiles for different indium concentrations (red: In = 0.25, blue: In = 0.30, and green: In = 0.35). The experimental and calculated relaxation profiles fit nicely for a QD composition of $In_{0.30}Ga_{0.70}As$. Claro *et al.* [26] already suggested that the WL of such InAlAs QDs might be Al rich, and the QDs could actually be made of $In_{0.50}Ga_{0.50}As$. However, these results were based on TEM results, where the size, geometry, and composition of the QDs were barely resolved, and on indirect band-structure calculations used to fit PL data. Obviously their lack of reliable structural information about the QDs themselves could dramatically affect the calculations and the final composition. Therefore, our analysis further supports the suggestion made by Claro *et al.* [26] that the Al atoms remain in the WL and are absent from the QDs. However, our topographic X-STM images provide much more accurate data about the morphology, size, and even composition of the nanostructures by combining X-STM with FE simulations. Consequently, we can conclude that the In content of such QDs should be even lower, and their composition is rather around $\sim In_{0.30}Ga_{0.70}As$.

The optical properties of all the layers were measured by PL at 77 K and their spectra are shown in Fig. 7. A single layer of conventional InAs QDs (layer 3) emits close to 1000 nm, whereas the spectrum of a single layer of InAlAs-QDs (layer 4) used as a seed is peaked around 875 nm due to their smaller size and lower In content. The PL intensity of the InAlAs QDs is much lower than that of InAs QDs as their ground state (the only confined state of the system) is closer to the top of the GaAs barriers. As a consequence, the confined carriers can easily escape due to the temperature used in the PL measurements (77 K). The narrow peak around 860 nm is related to their WL. Regarding the double layers of QDs, their PL spectra do not show any sign of the seed layer and seem to consist only of the emission from the top InAs QDs. This is due to the deeper ground state of the top InAs QDs where most carriers recombine, confirming that the seed layer is optically inactive in this kind of structure, as already seen before [25,26]. The PL spectra are slightly different for each type of double layers of QDs, as they result from the influence of the seed layer over the top InAs QDs, which should lead to an increase in their density and, consequently, to a reduction of their sizes with decreasing values of spacer thickness. However, due to the presence of strong indium segregation in the InAs/GaAs system, some of the indium atoms from the seed layer are also transferred to the top InAs

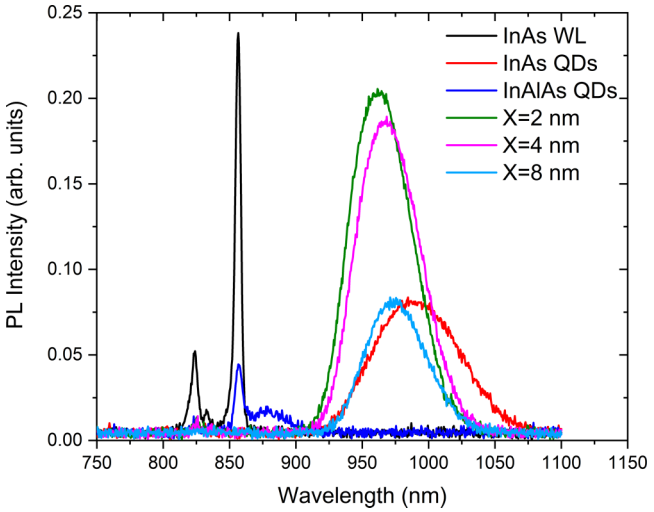

FIG. 7. PL spectra of all the layers measured at 77 K. The single layer of InAlAs QDs shows a weak emission close to 875 nm, and the single layer of InAs QDs emits around 1000 nm. All the double layers have a single emission between 950 and 1000 nm related to the top layer of InAs QDs, without any signal coming from the seed layer.

QDs, especially for thin GaAs spacers. This could be observed in the critical thickness (2D–3D transition observed on the RHEED screen) of the top InAs QDs, which was 1.7 MLs for the 8-nm-thick spacers, as in the single layer of InAs QDs of layer 3, but was reduced to 0.7 ML for the thinnest GaAs spacer (2 nm). However, when the spacer was reduced to 4 or 2 nm, the critical thickness was only 1.2 and 0.7 MLs, respectively, indicating that the top InAs QDs actually received more In atoms that were used to increase their size or In content. Therefore, when the spacer is reduced, the strain field acts to blueshift the emission, whereas, simultaneously, indium segregation acts in the opposite direction, yielding a redshift. The spectra resulting from this complex competition will depend on which of both effects prevails. The samples with the thinnest GaAs spacers (2 and 4 nm) have the highest PL intensity due to their larger QDs density, while the one with the thick spacer (8 nm) shows an intensity similar to the one of the single layer of InAs QDs, which is consistent with their similar QDs densities. The large band gap of the InAlAs WL (layer 2) was confirmed in our PL measurements, as the sample containing only 2.2 MLs of $In_{0.7}Al_{0.3}As$ (layer 2) showed no signal at all when excited with a laser having a wavelength of 660 nm, which corresponds to an energy of 1.878 eV. This value is much larger than the GaAs band gap at 77 K (1.503 eV) and suggests that the Al content of the WL is at least 30%, which is in good agreement with the X-STM and FE simulations. On the other hand, the 1.4-ML-thick InAs WL could be detected normally and appeared as a narrow peak around 855 nm.

It is clear from the X-STM images of the 2.2-ML-thick InAlAs layer [Fig. 3(b)] that the Al atoms remain at the bottom of the WL and only indium atoms segregate during deposition and capping. However, after the QDs formation, Fig. 4(b) revealed that all Al atoms still remain at the bottom of the WLs and the QDs are exclusively made of InGaAs without any trace of Al atoms. Therefore, unlike for InAs

QDs where the InGaAs WL lies around the QDs, in this particular case, the QDs in the InAlAs layer lies on top of an Al-rich WL. The FE simulations suggested that the Al-rich WL contains 30% of Al, and only 5%–10% of In, the rest being Ga atoms coming from the substrate or GaAs cap layer. Since only 2.2 MLs of InAlAs were deposited in layer 2 and the resolution of an X-STM image along the [001] direction is limited to a bilayer on a cleaved {110} surface, we cannot confirm if In segregation is stronger in InGaAs than in InAlAs [47]. However, from the topographic images shown in Fig. 3, the InAlAs WL (layer 2) appears to be thinner and In richer suggesting that the presence of Al atoms somehow pins more In atoms into the growth surface compared to InAs WL (layer 1). Surprisingly, there is no trace of Al atoms inside the InAlAs QDs, as already proposed by Claro *et al.* [26]. However, here we prove it directly with X-STM data, confirming that such InAlAs QDs are actually composed of InGaAs only, and their In content is even lower (around 30%–35%) than the value suggested by Claro *et al.* [26] (50%). It is thus now clear that the high density of QDs achieved during the deposition of InAlAs is not because they contain low mobility Al atoms which could generate a high density of nucleation centers but, instead, because the QDs are self-assembled on top of an Al-rich WL that provides low mobility to the In and Ga atoms and, consequently, generates a high density of small InGaAs islands. It is confirmed by other reports which showed that such a high density of In(Ga)As QDs could only be achieved when the In(Ga)As material was deposited on top of an AlAs surface [24,48]. Therefore, when simulating the optoelectronic properties of QDs formed from an $In_{0.7}Al_{0.3}As$ layer, the correct composition should be used ($In_{0.30}Ga_{0.70}As$ in our case) instead of the nominal one ($In_{0.7}Al_{0.3}As$). Another point that needs to be taken into account to provide accurate results is the much higher band gap of the WL that can strongly influence transport properties. Although it was estimated to contain around 30% of Al atoms in layer 2 of the X-STM sample investigated here, that value might eventually be higher after the formation of the QDs, as a larger amount of InAlAs is needed to effectively form the QDs, and these extra Al atoms will also be settled at the bottom of the WL. It is difficult to observe them in the X-STM images containing QDs, as the contrast from the QDs dominates and makes it harder to quantify the Al concentration in layer 4 and compare it with the Al concentration in layer 2.

Regarding the InAlAs/InAs QDs double layers, it is clear from the AFM and X-STM data that a 4-nm-thick GaAs spacer is highly effective in vertically aligning the InAs QDs in the top layer. The two QDs layers are completely intermixed, forming one large QD when the spacer is only 2 nm thick, but the density of InAs QDs in the top layer is even higher, and they continue dominating the optical properties of the system. GaAs spacers thicker than 8 nm are unable to provide any stacking, suggesting that the internal strain field is too weak to influence the nucleation of InAs QDs in the top layer. Although some X-STM images showed occasional stacking of two QDs, it is minor and is also typically observed in mechanically uncoupled double layers of QDs [49]. This distance (8 nm) is much smaller than the one usually found for double layers of InAs QDs (∼40–50 nm) [50]. It mainly results from the smaller size of the InAlAs QDs and their much lower In content which considerably weakens the local strain field [23]. The ideal seed layer is the one that can increase the density of InAs QDs in the top layer without interfering too much with their properties for a specific application [25,26]. In our case, the emission from the seed layer is absent in the PL spectra of the double layers of QDs, and the optical signal that is detected comes exclusively from the top InAs QDs. Since the growth conditions of the seed layer and top InAs QDs layers can be optimized separately, once the spacer thickness has been chosen to achieve the desired density of QDs in the top layer, it might even be possible to vary the amount of InAs material to be deposited in order to fine tune the emission of the QDs—here it was kept constant to 2.0 MLs.

IV. CONCLUSIONS

In summary, we performed a detailed structural characterization of a single layer of InAlAs QDs and their WL. Double layers of QDs were also investigated, where InAlAs QDs, which can be easily obtained with a high density, were used as a seed in an attempt to increase the density of InAs QDs deposited just a few nm above them. X-STM images of the InAlAs WL revealed that the Al atoms were confined within the bottom part, while the top part contained only In and Ga atoms. FE simulations based on the X-STM structural characterization suggested a composition of $In_{0.05–0.1}Al_{0.3}Ga_{0.60–0.65}As$ for the bottom part of the WL and $In_{0.65–0.70}Ga_{0.30–0.35}As$ for the top part. The In content in the top part of the WL was higher than expected, suggesting that In atoms may be pinned by the presence of the Al atoms on the surface. Regarding the QDs formed during deposition of the InAlAs alloy, X-STM also evidenced that they do not contain any Al atoms; they rather lie on top of the Al-rich part of the WL. FE calculations inferred that these QDs were actually made of $In_{0.30}Ga_{0.70}As$. Concerning the double layers of InAlAs and InAs QDs, the AFM analysis showed that the strain field generated by the high density of InAlAs QDs could effectively increase the density of InAs QDs in the top layer for very thin GaAs spacers (2–4 nm). For spacers thicker than 8 nm, the top InAs layer could no longer feel the influence of the seed layer, and its QDs density was the same as for a single InAs layer. X-STM data showed that the two QDs layers were completely intermixed for very thin spacers (2 nm). For intermediate spacers (4 nm), their QDs could be distinguished and were vertically aligned with some probability depending on their vertical separation. Both QDs layers were completely decoupled for a GaAs spacer of 8 nm and could thus be treated as individual layers. The optical properties of the double layers of QDs showed no emission from the seed, as expected for a good seed layer. An increase in the PL intensity of the InAs QDs and a small blueshift of their emission was detected for the smaller spacers, confirming the mechanical influence of the seed layer (higher InAs QDs density). Therefore, this detailed structural investigation provides new insights into the growth of single InAlAs QDs and double layers of InAlAs/InAs QDs. It sheds light on the position of the Al atoms in the InAlAs WLs and QDs, providing detailed feedback for fur-

ther growth optimization to improve the performance of the devices.

ACKNOWLEDGMENTS

This research was supported by the funding from the European Union's Horizon 2020 research and innovation program under the Marie Skłodowska-Curie, project 4PHOTON Grant Agreement No. 721394 and by funding from the Dutch Research Council (NWO) Zwaartekracht project on Integrated Nanophotonics with Project No. 10018478. This study was financed in part by the Coordenação de Aperfeiçoamento de Pessoal de Nível Superior - Brasil (CAPES) - Finance Code 001, and by the Conselho Nacional de Desenvolvimento Científico e Tecnológico, CNPq, Grant 311687/2017-2.

R.S.R.G, A.A.Q, and P.M.K conceived the original idea for this work. R.S.R.G and P.M.K performed X-STM experiments, FE simulations, and related analyses. A.A, V.M.O.C, and A.A.Q performed epitaxial growth, AFM, PL, and interpretation of the results. R.S.R.G wrote the manuscript and all the authors contributed to the overall scientific interpretation and editing of the manuscript. A.A.Q and P.M.K supervised this work.

The authors declare no conflicts of interest

[1] Q. Xie, A. Kalburge, P. Chen, and A. Madhukar, IEEE Photonics Technol. Lett. **8**, 965 (1996).
[2] Z. Chen, O. Baklenov, E. T. Kim, I. Mukhametzhanov, J. Tie, A. Madhukar, Z. Ye, and J. C. Campbell, J. Appl. Phys. **89**, 4558 (2001).
[3] N. López, A. Martí, A. Luque, C. Stanley, C. Farmer, and P. Diaz, J. Sol. Energy Eng. **129**, 319 (2007).
[4] M. Kroutvar, Y. Ducommun, J. J. Finley, M. Bichler, G. Abstreiter, and A. Zrenner, Appl. Phys. Lett. **83**, 443 (2003).
[5] E. M. Sala, I. F. Arikan, L. Bonato, F. Bertram, P. Veit, J. Christen, A. Strittmatter, and D. Bimberg, Phys. Status Solidi B **255**, 1800182 (2018).
[6] R. S. R. Gajjela, A. L. Hendriks, J. O. Douglas, E. M. Sala, P. Steindl, P. Klenovský, P. A. J. Bagot, M. P. Moody, D. Bimberg, and P. M. Koenraad, Light Sci. Appl. **10**, 125 (2021).
[7] A. J. Shields, Semiconductor quantum light sources, Nature Photonics **1**, 215 (2007).
[8] R. H. Hadfield, Nat. Photonics **3**, 696 (2009).
[9] R. S. R. Gajjela, N. R. S. van Venrooij, A. R. da Cruz, J. Skiba-Szymanska, R. M. Stevenson, A. J. Shields, C. E. Pryor, and P. M. Koenraad, Nanotechnology **33**, 305705 (2022).
[10] T. Müller, J. Skiba-Szymanska, A. B. Krysa, J. Huwer, M. Felle, M. Anderson, R. M. Stevenson, J. Heffernan, D. A. Ritchie, and A. J. Shields, Nat. Commun. **9**, 862 (2018).
[11] R. S. R. Gajjela, E. M. Sala, J. Heffernan, and P. M. Koenraad, ACS Appl. Nano Mater. **5**, 8070 (2022).
[12] D. Leonard, M. Krishnamurthy, C. M. Reaves, S. P. Denbaars, and P. M. Petroff, Appl. Phys. Lett. **63**, 3203 (1993).
[13] J. Belk, J. Sudijono, D. Holmes, C. McConville, T. Jones, and B. Joyce, Surf. Sci. **365**, 735 (1996).
[14] P. B. Joyce, T. J. Krzyzewski, G. R. Bell, B. A. Joyce, and T. S. Jones, Phys. Rev. B **58**, R15981 (1998).
[15] F. Ferdos, S. Wang, Y. Wei, M. Sadeghi, Q. Zhao, and A. Larsson, J. Cryst. Growth **251**, 145 (2003).
[16] F. Heinrichsdorff, A. Krost, M. Grundmann, D. Bimberg, A. Kosogov, and P. Werner, Appl. Phys. Lett. **68**, 3284 (1996).
[17] G. Capellini, L. Di Gaspare, F. Evangelisti, and E. Palange, Appl. Phys. Lett. **70**, 493 (1997).
[18] T. Asano, A. Madhukar, K. Mahalingam, and G. J. Brown, J. Appl. Phys. **104**, 113115 (2008).
[19] A. Lenz, H. Eisele, J. Becker, J.-H. Schulze, T. D. Germann, F. Luckert, K. Pötschke, E. Lenz, L. Ivanova, A. Strittmatter, D. Bimberg, U. W. Pohl, and M. Dähne, J. Vac. Sci. Technol. B **29**, 04D104 (2011).
[20] F. Hopfer, A. Mutig, M. Kuntz, G. Fiol, D. Bimberg, N. N. Ledentsov, V. A. Shchukin, S. S. Mikhrin, D. L. Livshits, I. L. Krestnikov, A. R. Kovsh, N. D. Zakharov, and P. Werner, Appl. Phys. Lett. **89**, 141106 (2006).
[21] A. Alzeidan, M. S. Claro, and A. A. Quivy, J. Appl. Phys. **126**, 224506 (2019).
[22] R. S. R. Gajjela, A. L. Hendriks, A. Alzeidan, T. F. Cantalice, A. A. Quivy, and P. M. Koenraad, Phys. Rev. Mater. **4**, 114601 (2020).
[23] A. Alzeidan, T. Cantalice, K. Vallejo, R. Gajjela, A. Hendriks, P. Simmonds, P. Koenraad, and A. Quivy, Sens. Actuators A **334**, 113357 (2022).
[24] P. Ballet, J. B. Smathers, and G. J. Salamo, Appl. Phys. Lett. **75**, 337 (1999).
[25] A. Kovsh, A. Zhukov, A. Egorov, V. Ustinov, Y. Shernyakov, M. Maximov, V. Volovik, A. Tsatsul'nikov, Y. Musikhin, N. Ledentsov, P. Kop'ev, D. Bimberg, and Z. Alferov, J. Cryst. Growth **201-202**, 1117 (1999).
[26] M. Claro, D. Stroppa, E. da Silva, and A. Quivy, Sens. Actuators A **315**, 112262 (2020).
[27] S. Gupta, P. K. Bhattacharya, J. Pamulapati, and G. Mourou, J. Appl. Phys. **69**, 3219 (1991).
[28] X. Z. Shang, S. D. Wu, C. Liu, W. X. Wang, L. W. Guo, Q. Huang, and J. M. Zhou, J. Phys. D **39**, 1800 (2006).
[29] X. Lu, Y. Izumi, M. Koyama, Y. Nakata, S. Adachi, and S. Muto, J. Cryst. Growth **322**, 6 (2011).
[30] L. Su, B. Liang, Y. Wang, Q. Guo, X. Li, S. Wang, G. Fu, Y. I. Mazur, M. E. Ware, and G. J. Salamo, Appl. Phys. Lett. **109**, 183103 (2016).
[31] A. Ben Daly, H. Riahi, F. Bernardot, T. Barisien, E. Galopin, A. Lemaître, M. Maaref, and C. Testelin, Superlattices Microstruct. **104**, 321 (2017).
[32] R. Kuszelewicz, J.-M. Benoit, S. Barbay, A. Lemaître, G. Patriarche, K. Meunier, A. Tierno, and T. Ackemann, J. Appl. Phys. **111**, 043107 (2012).
[33] X. Lu, M. Koyama, Y. Izumi, Y. Nakata, S. Adachi, and S. Muto, Jpn. J. Appl. Phys. **52**, 025602 (2013).
[34] C. F. Schuck, R. Boutelle, K. Silverman, G. Moody, and P. J. Simmonds, J. Phys. Photonics **3**, 024012 (2021).
[35] S. Golovynskyi, O. I. Datsenko, L. Seravalli, G. Trevisi, P. Frigeri, B. Li, D. Lin, and J. Qu, Microelectron. Eng. **238**, 111514 (2021).
[36] I. Mukhametzhanov, R. Heitz, J. Zeng, P. Chen, and A. Madhukar, Appl. Phys. Lett. **73**, 1841 (1998).

[37] R. M. Feenstra, J. A. Stroscio, J. Tersoff, and A. P. Fein, Phys. Rev. Lett. **58**, 1192 (1987).
[38] S. Koshiba, Y. Nakamura, M. Tsuchiya, H. Noge, H. Kano, Y. Nagamune, T. Noda, and H. Sakaki, J. Appl. Phys. **76**, 4138 (1994).
[39] R. Feenstra, Phys. B: Condens. Matter **273-274**, 796 (1999).
[40] R. M. Feenstra, Semicond. Sci. Technol. **9**, 2157 (1994).
[41] J. Moison, F. Houzay, F. Barthe, J. Gérard, B. Jusserand, J. Massies, and F. Turco-Sandroff, J. Cryst. Growth **111**, 141 (1991).
[42] J. G. Keizer, J. Bocquel, P. M. Koenraad, T. Mano, T. Noda, and K. Sakoda, Appl. Phys. Lett. **96**, 062101 (2010).
[43] R. S. R. Gajjela and P. M. Koenraad, Nanomaterials **11**, 85 (2021).
[44] J. Ibáñez, R. Cuscó, L. Artús, M. Henini, A. Pataè, and L. Eaves, Appl. Phys. Lett. **88**, 141905 (2006).
[45] A. Sahli, H. Helali, A. Melliti, A. Moadhen, M. A. Maaref, M. Oueslati, and A. Lemaître, Silicon **11**, 2471 (2019).
[46] See the Supplemental Material at http://link.aps.org/supplemental/10.1103/PhysRevMaterials.6.114604 for finite element simulations.
[47] J. M. Gerard, Appl. Phys. Lett. **61**, 2096 (1992).
[48] P. Offermans, P. M. Koenraad, J. H. Wolter, K. Pierz, M. Roy, and P. A. Maksym, Phys. Rev. B **72**, 165332 (2005).
[49] Q. Xie, A. Madhukar, P. Chen, and N. P. Kobayashi, Phys. Rev. Lett. **75**, 2542 (1995).
[50] M. O. Lipinski, H. Schuler, O. G. Schmidt, K. Eberl, and N. Y. Jin-Phillipp, Appl. Phys. Lett. **77**, 1789 (2000).